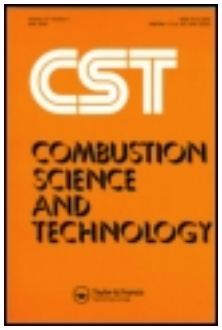


Combustion Science and Technology
Publication details, including instructions for authors and subscription information:
http://www.tandfonline.com/loi/gcst20

# Numerical Analyses for Radiative Autoignition and Transition to Flame Spread over a Vertically Oriented Solid Fuel in a Gravitational Field

PEI-HSUN LIN [a] & CHIUN-HSUN CHEN [a]
[a] Department of Mechanical Engineering , National Chiao-Tung University , HsinChu, Taiwan, 30050, R.O.C
Published online: 24 Oct 2007.

To cite this article: PEI-HSUN LIN & CHIUN-HSUN CHEN (2000) Numerical Analyses for Radiative Autoignition and Transition to Flame Spread over a Vertically Oriented Solid Fuel in a Gravitational Field, Combustion Science and Technology, 151:1, 157-187, DOI: 10.1080/00102200008924218

To link to this article: http://dx.doi.org/10.1080/00102200008924218

*Combust. Sci. and Tech.*, 2000, Vol. 151, pp. 157-187
Reprints available directly from the publisher
Photocopying permitted by license only





# Numerical Analyses for Radiative Autoignition and Transition to Flame Spread over a Vertically Oriented Solid Fuel in a Gravitational Field

PEI-HSUN LIN and CHIUN-HSUN CHEN*

*Department of Mechanical Engineering, National Chiao-Tung University, HsinChu, Taiwan 30050, R.O.C*

*(Received December 08, 1998; Revised April 28, 1999)*

This study numerically investigates the ignition behaviors of vertically oriented cellulosic materials subjected to a radiant heat flux in a normal gravitational field. The entire process is delineated into two distinct stages. In the heating up stage, the maximum temperature increases with time but at a decreasing rate because of the pyrolysis reaction. The flame development stage consists of ignition and transition processes. In the ignition process, the maximum temperature in gas phase increases dramatically within a short period of time because a large amount of heat is generated from chemical reaction of the accumulative, flammable mixture. The flame is in a transition from a premixed flame to a diffusion one, except for the small region around the flame front. For the effect of varying the heating duration on ignition behavior, prolonging the imposed radiative heat time leads the ignition from a transition one to a persisting ignition. The effect of varying the solid fuel thickness indicates that the ignition delay time increases with an increase of solid fuel thickness while $\delta_s \leq 1.802$. For $1.802 \leq \delta_s \leq 3.244$, the ignition delay times remain constant. Finally, if the external heating rate is the same order as the heat diffuse rate, the ignition delay time increases with an increase in solid fuel thickness.

*Keywords:* Ignition; Flame Spread

## INTRODUCTION

This study investigates the ignition and transition to flame spread behaviors of a vertically oriented solid fuel subjected to a radiant heat flux under a natural con-

* Corresponding Author: Chiun-Hsun Chen, Department of Mechanical Engineering, National Chiao-Tung University, HsinChu, Taiwan 30050, R.O.C. Telephone : 886-3-5712121 Ext 55130, FAX : 886-3-5721091, E-mail: chchen@cc.nctu.edu.tw

vective environment in a normal gravitational field. Although this process plays an important role in natural fire growth, previous modeling studies of solid fuel ignition phenomena only considered the following topics: simple flow fields, such as stagnation point flow (Amos and Fernandez-Pello, 1988) and potential flow in microgravity environment (Nakabe et al., 1994; Mcgrattan et al., 1996); solid fuel energy conservation (Bradley, 1970); and one-dimensional assumptions (Kashiwagi, 1974; Kindelan and Williams, 1977; Gandhi and Kanury, 1988). No sophisticated models are available to describe the detailed interaction between the gas phase transport/chemical process and the solid fuel heating/pyrolysis process. In addition, most previous works studied ignition and flame spread phenomena separately. Relatively few works, including Nakabe et al. (1994) and Mcgrattan et al. (1996), investigated the transition process from ignition to flame spread. This work concentrates mainly on establishing a more complete combustion model to study the detailed process for ignition and subsequent flame spread over a thick solid fuel.

Martin (1965) demonstrated that the radiative ignition behaviors of vertical cellulosic sheets can be divided into three regions according to the incident irradiance. Convection heat loss and diffusion of heat into the solid fuel are the main control mechanisms for low- and middle-level irradiance, respectively. For high-level irradiance, deposition is limited to the material very near the exposed surface: ablation is the most important effect. Similarly, Alvares and Martin (1971) indicated that ignition time decreases as the ambient oxygen concentration or the total pressure increases beyond its ignition limiting value.

Kashiwagi (1979a, 1979b, and 1981) pointed out that the plume of decomposing products strongly attenuates radiation. His experimental results (Kashiwagi, 1979a) confirmed that the energy absorbed by decomposing products attenuates the incident radiant heat flux by up to 80%. In addition, the spontaneous ignition of PMMA can only occur by absorbing energy from incident radiation in the gas phase if the radiation intensity exceeds a value of 16 $W/cm^2$. According to results for horizontally- (Kashiwagi, 1979b) and vertically-mounted (Kashiwagi, 1981) PMMA and red oak sheets, such an effect impacts surface temperature at ignition, indicating that surface temperature at ignition depends on the specified condition (including the material itself).

Kashiwagi (1974) concluded that the in-depth absorption of an incident radiation by solid fuel affects the ignition delay time for plastic materials. In addition, parametric studies of activation energy revealed a finite range of activation energy, for both gas and solid phase, within which solid fuel can be ignited. Numerical analyses of Bradley (1970) and Gandhi and Kanury (1988) conferred with that observation.

Nakabe et al. (1994) developed an axisymmetric, time-dependent model to describe the autoignition and flame spread phenomena of a thermally-thin cellulosic material in a quiescent microgravity environment. According to their results, autoignition occurs with a 30% of oxygen concentration, and the transition from ignition to flame spread does not occur until the oxygen concentration reaches 50%.

Mcgrattan et al. (1996) investigated radiative ignition and the subsequent transition to flame spread over a thermally-thin cellulosic material in a microgravity environment. In their study, ignition started away from either end of the sample. Calculation results agreed with the experimental data obtained in a 2.2-s drop tower. Both results indicated that an imposed wind up to 5cm/s enhances the strength of the opposed flame spread rate due to the greater supply of oxygen; the downstream flame front tends to diminish during the transition period as well. In addition, their results further demonstrated that the ignition delay time depends mainly on the peak flux of external radiation. Meanwhile, the transition time to flame spread, because of the preheating effect, depends mainly on the broadness of the flux distribution.

In light of above developments, this study develops a time-dependent combustion model to simulate and study the process of radiative autoignition and subsequent transition to flame spread over a vertically oriented solid fuel. The parametric studies change the solid fuel thickness ranging from the thermally-thin to thermally-thick fuels, the peak values of externally imposed flux values, and the heating periods. This study concentrates mainly on providing further insight into the detailed ignition processes and their respective controlling mechanisms.

## MATHEMATICAL MODEL

Figure 1 illustrates the physical configuration of two-dimensional ignition over a vertically oriented solid fuel. At time $t < 0$, the system is quiescent. When $t \geq 0$, an external heat flux in Gaussian distribution is imposed on the solid surface. Next, the solid is heated up and its temperature rises, and, subsequently, pyrolysis occurs. Meanwhile, the hot surface transfers heat to the gas layer adjacent to it. A rise in the gas phase temperature causes a change in density; the resulting fluid motion builds a natural convection near the fuel plate. However, this flow field cannot be prescribed in advance but provided as part of the solution. The detailed mathematical model, including both gas and solid phases to describe the whole process mentioned above, will be given later.

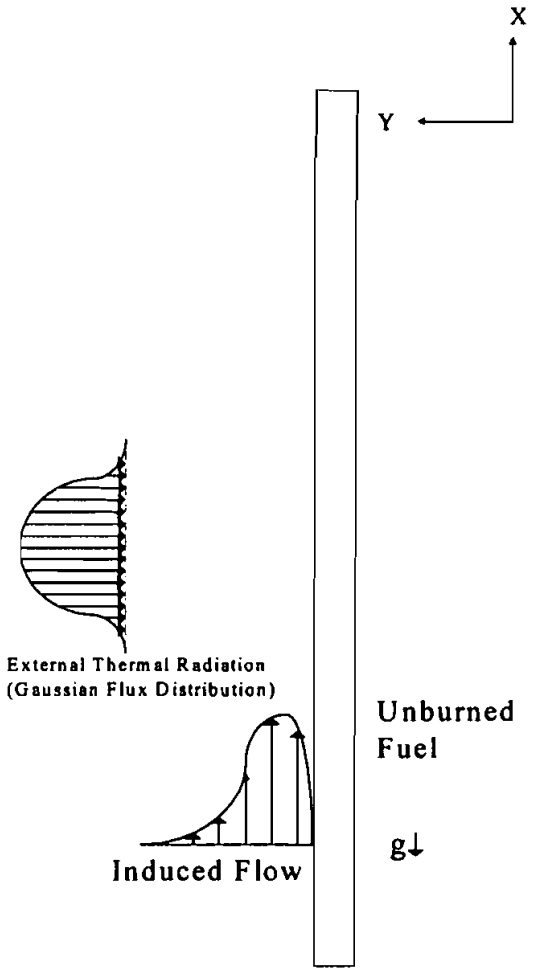


FIGURE 1 Configuration of radiative ignition of a vertically-oriented solid fuel

The assumptions for the combustion model are essentially the same as those proposed in a previous study that investigated the behavior of a downward flame spread for cellulosic materials (Lin and Chen, 1999), except that, the time-dependent conservation equations are considered herein. Although this study explores the radiative autoignition of a solid fuel, the gas phase absorption of external radiative energy is not considered in gas phase model because of the following reasons. First, as mentioned in Introduction section, gas phase radiation absorption is important only when the radiation intensity surpassesa value of

16 W/cm$^2$ (Kashiwagi, 1979a), whereas the peak heat flux applied herein ranges between 5 to 6.5 w/cm$^2$. As expected, the effect of radiation absorption is only slight. This statement is also confirmed by Fernandez-Pello (1995) that radiation absorption affects ignition behavior only when the radiation intensity exceeds a certain minimum (of the order of 60 W/cm$^2$). These radiant fluxes are too large to be expected in a normal fire. Second, the radiation absorption in gas phase strongly depends on the wavelength emitted by heat source. Restated, radiation absorption is not an important factor for most radiation heat sources, whose spectrum is not specified for absorption. For example, if a tung-sten lamp is used as the heat source, which emits the majority of its energy in the near infrared, the radiation absorption in gas phase will be reduced as much as possible during the ignition period (Mcgrattan et al., 1996).

This model solves the system of governing equations non-dimensionally. The detailed normalization procedure can be found in Lin (1998). Table I summarizes the dimensionless, unsteady governing equations for continuity, momentum, energy, and species in gas phase.

TABLE I Gas phase governing equations

$$\frac{\partial}{\partial t}(\rho\phi) + \frac{\partial}{\partial x}\left(\rho u\phi - \Gamma\frac{\partial\phi}{\partial x}\right) + \frac{\partial}{\partial y}\left(\rho v\phi - \Gamma\frac{\partial\phi}{\partial y}\right) = S$$

| *Equation* | $\phi$ | $\Gamma$ | $S$ |
|---|---|---|---|
| continuity | 1 | – | 0 |
| x-momentum | u | $\frac{\mu}{\sqrt{Gr}}$ | $\frac{\partial P}{\partial x} + S_u + \frac{\rho_\infty - \rho}{\rho_\infty - \rho_f}$ |
| y-momentum | V | $\frac{\mu}{\sqrt{Gr}}$ | $\frac{\partial P}{\partial y} + S_v$ |
| energy | T | $\frac{\mu}{Pr\cdot\sqrt{Gr}}$ | $-q\cdot\dot{\omega}_F$ |
| fuel | $Y_F$ | $\frac{\mu}{Pr\cdot\sqrt{Gr}\cdot Le}$ | $\dot{\omega}_F$ |
| oxidizer | $Y_O$ | $\frac{\mu}{Pr\cdot\sqrt{Gr}\cdot Le}$ | $f\cdot\dot{w}_F$ |

$$S_u = \frac{1}{3}\frac{\partial}{\partial x}\left(\frac{\mu}{\sqrt{Gr}}\frac{\partial u}{\partial x}\right) + \frac{\partial}{\partial y}\left(\frac{\mu}{\sqrt{Gr}}\frac{\partial v}{\partial x}\right) - \frac{2}{3}\frac{\partial}{\partial x}\left(\frac{\mu}{\sqrt{Gr}}\frac{\partial v}{\partial y}\right)$$

$$S_v = \frac{1}{3}\frac{\partial}{\partial y}\left(\frac{\mu}{\sqrt{Gr}}\frac{\partial v}{\partial y}\right) + \frac{\partial}{\partial x}\left(\frac{\mu}{\sqrt{Gr}}\frac{\partial u}{\partial y}\right) - \frac{2}{3}\frac{\partial}{\partial y}\left(\frac{\mu}{\sqrt{Gr}}\frac{\partial u}{\partial x}\right)$$

The conservation equations for solid phase are formulated as follows:
Conservation of mass:

$$\frac{\partial \rho_s}{\partial t} = -\left(\frac{A_s}{\delta_s}\right)\left(\frac{\rho_s - \rho_{sf}}{1-\rho_{sf}}\right)\exp\left(-\frac{E_s}{T_s}\right) \tag{1}$$

Conservation of energy:

$$\rho_s \frac{\partial T_s}{\partial t} = \frac{\partial m_s''}{\partial y}\cdot\delta_s\cdot[L+(1-C)(T_s-1)] + \alpha_s\frac{\partial^2 T_s}{\partial x^2} + \alpha_s\frac{\partial^2 T_s}{\partial y^2} - (C\cdot m_s''\cdot\delta_s)\frac{\partial T_s}{\partial y} \tag{2}$$

The boundary conditions for both gas- and solid-phase governing equations are

*Gas Phase*

$$\text{At } x = x_{min}:$$
$$u \cong 0, \quad v \cong 0, \quad T = 1, \quad Y_F = 0, \quad Y_O = Y_{O\infty} \tag{3}$$

$$\text{At } x = x_{max}:$$
$$\frac{\partial u}{\partial x} = \frac{\partial v}{\partial x} = \frac{\partial T}{\partial x} = \frac{\partial Y_F}{\partial x} = \frac{\partial Y_O}{\partial x} = 0 \tag{4}$$

$$\text{At } y = y_{max}:$$
$$\frac{\partial u}{\partial y} = 0, \quad \frac{\partial v}{\partial y} = 0, \quad T = 1, \quad Y_F = 0, \quad Y_O = Y_{O\infty} \tag{5}$$

*Solid phase*

$$\text{At } x = x_{min}:$$
$$T_s = 1 \tag{6}$$

$$\text{At } x = x_{max}:$$
$$\frac{\partial T_s}{\partial x} = 0 \tag{7}$$

At the mid-plane of the solid fuel bed:

$$\left.\frac{\partial T_s}{\partial y}\right|_{y=0} = 0 \tag{8}$$

The gas-phase equations are coupled with the solid-phase energy and mass conservation equations at the interface. Their relations are

$$T_i = T_{si}, \; k_s \left.\frac{\partial T_{si}}{\partial y}\right|_{y=\delta_s} = \mu \left.\frac{\partial T_i}{\partial y}\right|_{y=\delta_s} + q_{ext} + \sigma\varepsilon(T_s^4 - T_\infty^4),$$

$$u = 0, \; m_s'' = \rho_i v_i$$

$$m_i'' Y_{Fs} = m_i'' Y_{Fi} - \frac{\mu}{Pr\sqrt{Gr}Le}\cdot\left.\frac{\partial Y_F}{\partial y}\right|_{y=\delta_s}$$

$$m_i'' Y_{Os} = m_i'' Y_{Oi} - \frac{\mu}{Pr\sqrt{Gr}Le}\cdot\left.\frac{\partial Y_O}{\partial y}\right|_{y=\delta_s}, \text{ where } Y_{Fs} = 1, \; Y_{Os} = 0 \tag{9}$$

Notably, a radiation loss term is included at interface.

The numerical scheme adopts the SIMPLE algorithm (Patankar, 1980) and was thoroughly described by Lin (1998). Table II summarizes the results of time-step and grid independence tests for the case of non-dimensional solid fuel thickness $\delta_s$=1.802 (corresponding to 2.5mm). According to this table, the solution obtained by the grid distribution of 230 × 89 (corresponding to a nondimensional computational domain of 444.5 × 133.5) with a time step $\Delta t = 10$ (equal to 0.0548 sec. dimensionally) is acceptable; this set is also an optimal combination for the following computations. An SGI INDIGO2 workstation, located at National Chiao Tung University, performed the computations. The execution time for a typical case is about three hours.

TABLE II Grid and time step test results

| *Grid Number* ($x \times y$) | *Computational Domain (non-dimensional)* | *Time Step (non-dimensional)* | *Non-dimensional Ignition Delay Time* |
|---|---|---|---|
| 239×119 | 471.5×133.5 | 10.0 | 770.0 |
| 230×119 | 466.2×143. 1 | 10.0 | 770.0 |
| 230×119 | 444.5×133.5 | 10.0 | 770.0 |
| 230×109 | 444.5×103.5 | 10.0 | 770.0 |
| 230×119 | 392.6×117.0 | 10.0 | 770.0 |
| 230×129 | 444.5×163.5 | 10.0 | 770.0 |
| 220×119 | 414.3×133.5 | 10.0 | 770.0 |
| 230×119 | 444.5×133.5 | 7.5 | 772.5 |
| 230×119 | 444.5×133.5 | 10.0 | 770.0 |
| 230×119 | 444.5×133.5 | 15.0 | 762.5 |
| 230×119 | 444.5×133.5 | 30.0 | 780.0 |

## RESULTS AND DISCUSSION

The selected solid fuel is a cellulosic material. Table III lists all the properties describing gas phase chemical reaction and processes for solid fuel pyrolysis. They are the same as those used in a previous study that investigated the behavior of downward flame spread for cellulosic materials (Lin and Chen, 1999). Table IV presents the non-dimensional parameters derived by normalizing this governing system. This work first elucidates the ignition mechanisms of a vertical oriented solid fuel under natural convection environment in a normal gravitational field. It follows the parametric studies based on the variations of the incident heat flux duration, solid fuel thickness, and peak heat flux value.

TABLE III Gas and solid properties

| *Symbol* | *Units* | *Value* | *Reference* |
|---|---|---|---|
| $\overline{E}_s$ | J/mole | $1.396 \times 10^5$ | West et al.(1992) |
| $\overline{A}_s$ | 1/sec | $5 \times 10^{10}$ | West et al.(1992) |
| $\overline{L}$ | J/g | −795 | Di Blasi et al. (1988) |
| $\overline{k}_s$ | W/cm K | $1.325 \times 10^{-3}$ | Di Blasi et al. (1988) |
| $\overline{C}_s$ | J/g K | 1.325 | Di Blasi et al. (1988) |
| $\overline{\rho}_{s\infty}$ | g/cm$^3$ | 0.28 | Suzuki et al. (1994) |
| $\overline{T}_v$ | k | 700 | Di Blasi et al. (1994) |
| f | – | 1.185 | Altenkirch et al. (1980) |
| $\overline{R}$ | J/mole·K | 8.314 | Natl. Bur. Stan. (1955) |
| $\overline{C}_p$ | J/g·K | $f(\overline{T}^*)$ | Natl. Bur. Stan. (1955) |
| $Y_{O\infty}$ | – | 0.233 | Altenkirch et al. (1980) |
| $\overline{\rho}^*$ | g/cm$^3$ | $f(\overline{T}^*)$ | Natl. Bur. Stan. (1955) |
| $\overline{\alpha}^*$ | cm$^2$/sec | $f(\overline{T}^*)$ | Natl. Bur. Stan. (1955) |
| $\overline{T}_\infty$ | K | 298 | Altenkirch et al. (1980) |
| $\overline{T}_f$ | K | 2822 | Altenkirch et al. (1980) |
| $\overline{k^*}$ | W/cm·K | $f(\overline{T}^*)$ | Natl. Bur. Stan. (1955) |
| $\overline{\mu^*}$ | g/cm·sec | $f(\overline{T}^*)$ | Natl. Bur. Stan. (1955) |
| $\overline{E}$ | J/mole | $8.720 \times 10^4$ | Duh (1991) |
| $\overline{B}$ | cm$^3$/mole·sec | $1.00 \times 10^{12}$ | Altenkirch et al. (1980) |

Previous investigators have proposed many criteria to define when ignition occurs, such as critical surface temperature by Martin (1965). However, the uncertainty still exists. Various ignition criteria for condense fuel were reviewed by Kashiwagi (1974) and Kanury (1995). Ignition occurs when the gas phase temperature rises rapidly due to a rapid exothermic oxidizer reaction. Therefore, this work defines ignition to initiate as soon as the chemical reaction rate in gas phase exceeds $10^{-4}$ g/cm$^3$.s. This adopted definition is the same as that defined for a flame in Nakabe et al. (1994).

TABLE IV Non-dimensional parameters

| *Symbol* | *Parameter group* | *Value* |
|---|---|---|
| Pr | $\overline{\nu}/\overline{\alpha}$ | 0.705 |
| Le | $\overline{\alpha}/\overline{D}$ | 1.000 |
| Gr | $\overline{g}(\overline{\rho_\infty}-\overline{\rho_f})\overline{\delta}^3/\overline{\rho^*}\overline{\nu^*}^2$ | 1.424 |
| Da | $B\overline{\rho^*}\overline{\delta}/\overline{V_r}$ | $1.234\times10^6$ |
| C | $\overline{C_p}/\overline{C_s}$ | 0.938 |
| $\gamma$ | $\overline{T^*}/\overline{T_\infty}$ | 5.235 |
| $T_V$ | $\overline{T_v}/\overline{T_\infty}$ | 2.349 |
| E | $\overline{E}/\overline{RT_\infty}$ | 35.196 |
| q | $\overline{q}/\overline{c_p}\overline{T_\infty}$ | 45.224 |
| $\rho_{sf}$ | $\overline{\rho_{sf}}/\overline{\rho_{s\infty}}$ | 0.070 |
| $k_S$ | $\overline{k_s}/\overline{k^*}$ | 0.743 |
| L | $\overline{L}/\overline{c_s}\overline{T_\infty}$ | −2.013 |
| $A_s$ | $\overline{A_s\alpha^*}/\overline{V_r}^2$ | $2.738\times10^8$ |
| $E_S$ | $\overline{E_s}/\overline{RT_\infty}$ | 56.345 |

## Radiative Ignition Process

This work illustrates the radiative flaming ignition process using a solid fuel thickness of $\delta_s$=1.802 (Case (G) in Table V) as the reference case. According to Kashiwagi (1981), there are two modes for such an ignition: autoignition and piloted ignition. It is the former mode in this work. The selected thickness is regarded as a thermally-thick solid fuel from the finding of our recent work (Lin and Chen, 1999). The half-width of the externally imposed Gaussian heat flux distribution is 1cm wide (corresponding to 7.2 nondimensionally) with a peak value of 5 W/cm$^2$. The specified ambient mass fraction of oxygen is 0.233.

Figures 2~7 demonstrate the radiative flaming ignition and transition to the flame spread processes. The whole process is divided into two distinct stages

according to the relationship between maximum temperature and time as shown in Fig. 2: (I) Heating up stage, and (II) Flame development stage.

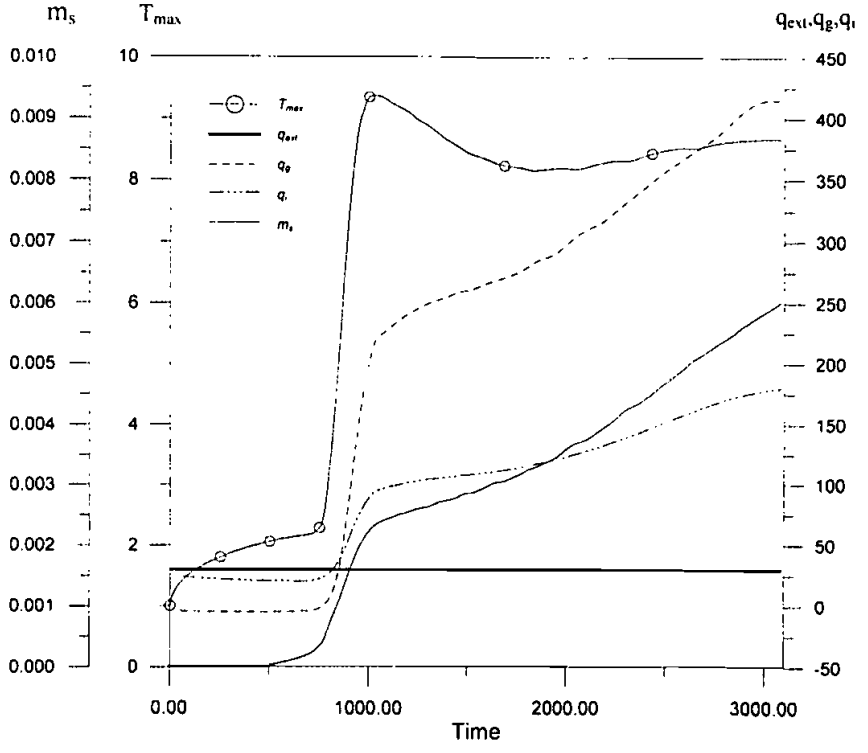


FIGURE 2 Time history for maximum temperature($T_{max}$), total externally imposed heat flux ($q_{extt}$), total heat flux received at interface originated from gas phase ($q_g$), total net interface heat flux received by solid fuel($q_i$) and mass flux($m_s$)

The first stage begins when the external radiative heat flux starts to impose on the fuel surface, and ends as the ignition to occur. The flame development stage includes both the ignition and transition processes. The ignition process starts from ignition initiation. The transition process starts when the maximum temperature reaches its highest value.

The time interval of heating up stage is $0 \leq t < 770$, in which the upper limit is the time for ignition initiation. The duration, 770, is defined as the non-dimensional ignition delay time (I.D.T.) for the specified conditions. Figure 2 reveals that the maximum temperature increases with time during this stage. Cases (a) and (b) in Figs. 3 to 5 demonstrate the heating up process.

TABLE V Parameteric study (Effect of changing solid fuel thickness)

| *NO.* | $\overline{\delta}_s$(mm) | $\delta_s$ | *I.D.T* | $T_{simax}$ | $\delta_c$ |
|---|---|---|---|---|---|
| A | 0.50 | 0.360 | 290 | 2.25 | 0.470 |
| B | 0.75 | 0.541 | 410 | 2.27 | 0.704 |
| C | 1.00 | 0.721 | 520 | 2.25 | 0.939 |
| D | 1.25 | 0.901 | 600 | 2.27 | 1.173 |
| E | 1.50 | 1.082 | 670 | 2.25 | 1.408 |
| F | 2.00 | 1.442 | 730 | 2 26 | 1.877 |
| G | 2.50 | 1.802 | 770 | 2.26 | 2.347 |
| H | 3.00 | 2.163 | 770 | 2.25 | 2.816 |
| I | 3.50 | 2.523 | 770 | 2.26 | 3.286 |
| J | 4.00 | 2.884 | 770 | 2.25 | 3.755 |
| K | 4.50 | 3.244 | 770 | 2.26 | 4.224 |
| L | 5.00 | 3.605 | 790 | 2 25 | 4.694 |

Figures 3(a) and 5(a) reveal that both gas and solid phase temperatures rise at t=190 after radiative heat is externally imposed on the interface. The computed non-dimensional maximum temperature ($T_{max}$) is located at the interface, with a value of 1.72. Herein, we define the heated region as the enclosure surrounded by the temperature in gas phase or solid fuel greater than 1.1, and the heat penetration depth as the vertical length measured from the interface to where $T_S$=1.1. Correspondingly, the maximum non-dimensional heat penetration depth is 0.8 at this instant. Since the external heat flux is a Gaussian distribution and the peak is located at x=0, as expected, the maximum heat penetration depth is located at x=0 and the constant temperature contours in solid show an arc shape. Our results also demonstrate that the temperature distribution in both gas and solid fuel is nearly symmetrical about x=0, implying that the heat transfer caused by convection is not significant. Regarding the flow structure (Fig. 3(a)), the arising buoyant force, originating from the density variation of the heated gas layer adjacent to the fuel surface, leads to an entrainment flow from the initial quiescent ambient. The maximum non-dimensional induced flow velocity is 0.216. Owning to the buoyancy effects, the entrained flow dominantly moves upward (toward + x); however, the movement can only be sustained when the buoyancy effect remains stronger than the viscous effect (to about x=10, where the flow becomes almost quiescent). In addition, the flow is deflected outward (towards +y, in the vicinity of x=5) because of thermal expansion. The distributions of fuel/oxygen mass fraction in Fig 4(a) demonstrate that almost all the oxygen mass fraction remains as in its the ambient value, i.e., $Y_{o\infty}$=0.233. This finding implies that the pyrolysis in the solid fuel is not yet active at this moment.

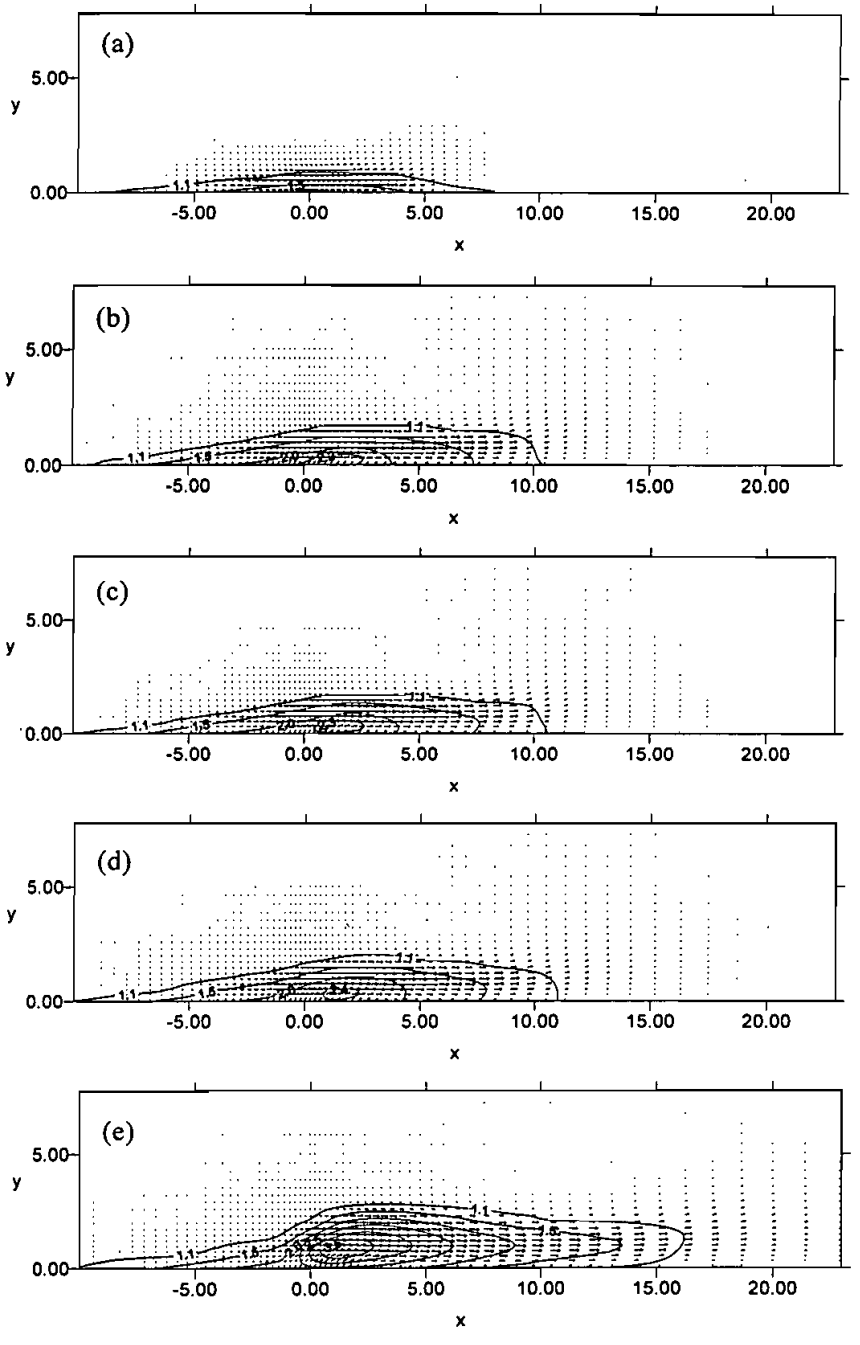

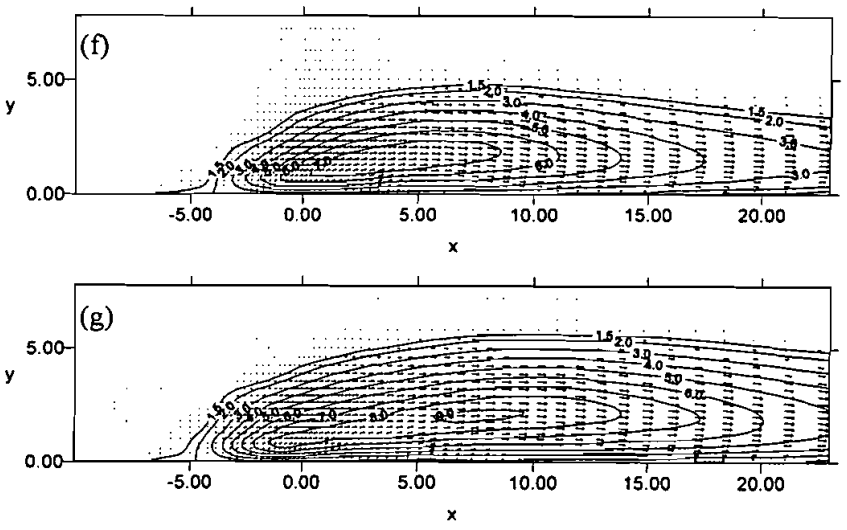


FIGURE 3 Isotherm and velocity vector distributions for (a) t=190 (b) t=760 (c) t=770 (d) t=780 (e) t=820 (f) t=920 (g) t=1030

At t=760 (the instant immediately before gas phase ignition occurs), a wider and deeper portion of the solid fuel becomes affected by the externally imposed heat flux because of continuous heating; as shown in Fig. 5(b). The heated region in gas phase expands (Fig. 3(b)) as well. For the related flow structure, the expansion of gas phase heated region causes the flow induced region to be enlarged, and further accelerates the induced flow velocity; the maximum velocity increases to 0.704 at t=760. Notably, the gas phase temperature distribution becomes less symmetrical around x=0, and the heated area is further extended downstream because of the stronger heat convection. Upstream, the induced ambient-temperature air flow cools the heated gas. Downstream, the accelerated/deflected gas flow brings the heat outward and further expands the heated region there. Besides, the volatile compounds released from the pyrolyzed solid fuel diffused and convected outward to mix with ambient air, diluting the oxygen concentration and forming a premixed fuel/oxygen mixture adjacent to the pyrolyzing surface (Fig. 4(b)). The resulting distribution of fuel mass fraction is mainly affected by flow motion, and the volatile compounds are carried downstream by convection. The gas phase maximum temperature (=2.33) now surpasses the maximum temperature at the interface (= 2.23), indicating that the weak chemical reactions have occurred in gas phase near the interface. Although too weak to form a flame, these reactions can still increase the gas phase temperature and, subsequently, further activate the chemical reactions.

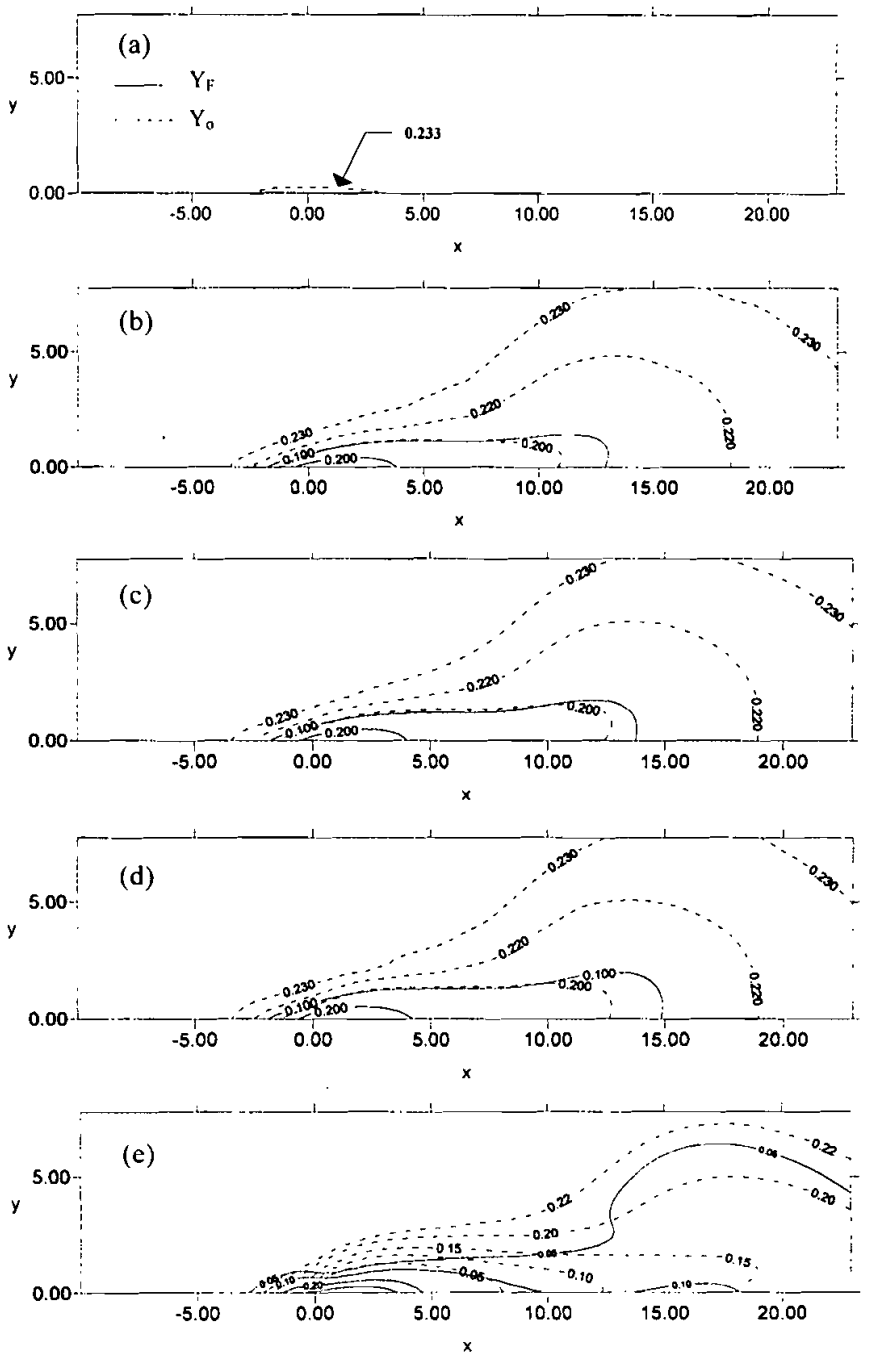

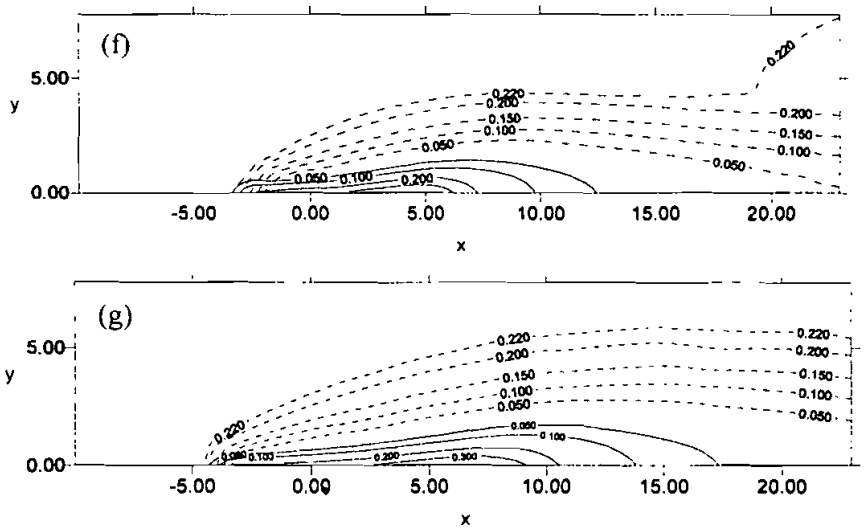


FIGURE 4 Fuel and oxygen mass fraction contours for (a) t=190 (b) t=760 (c) t=770 (d) t=780 (e) t=820 (f) t=920 (g) t=1030

At the interface, the averaged temperature increase rate is 126.6K/s for the first 2.36 seconds (t=0 to 430), and then followed by 37.5K/s from t=430 to t=760. The distinct characteristics in the heating process are largely owing to pyrolysis reaction in the solid fuel. Figure 6 confirms this feature by demonstrating that the pyrolyzed region, defined as the region where $\rho_s \leq 0.99$, is significantly larger at t=760 than it was before t=430, where the pyrolysis is not detectable yet. Restated, in addition to heating the solid fuel for the initial stage, the external imposed heat also contributes to the energy required by the endothermic pyrolysis process. Meanwhile, the outward motion of volatiles carries heat out, further retarding the heating of solid fuel. The thermal equilibrium for solid fuel during this period is the balance between externally imposed energy, surface radiation loss, endothermic gasification reaction, conduction, and internal convection energy within the solid fuel. It resembles what is defined by Kindelan and Williams (1977) as the transition stage. On the other hand, the period before t=430 is exactly like that defined by the last reference also as the inert stage, in which the received energy mainly heats the inner part of solid fuel by conduction; a faster-rising maximum temperature is the result.

While considering interface conditions, Fig. 2 also depicts that, in the heating up stage, the total net energy received $(q_{ij}(= \int_{x=x_{min}}^{x=x_{max}} k \left.\frac{\partial T}{\partial y}\right|_{y=\delta_s^-} dx))$

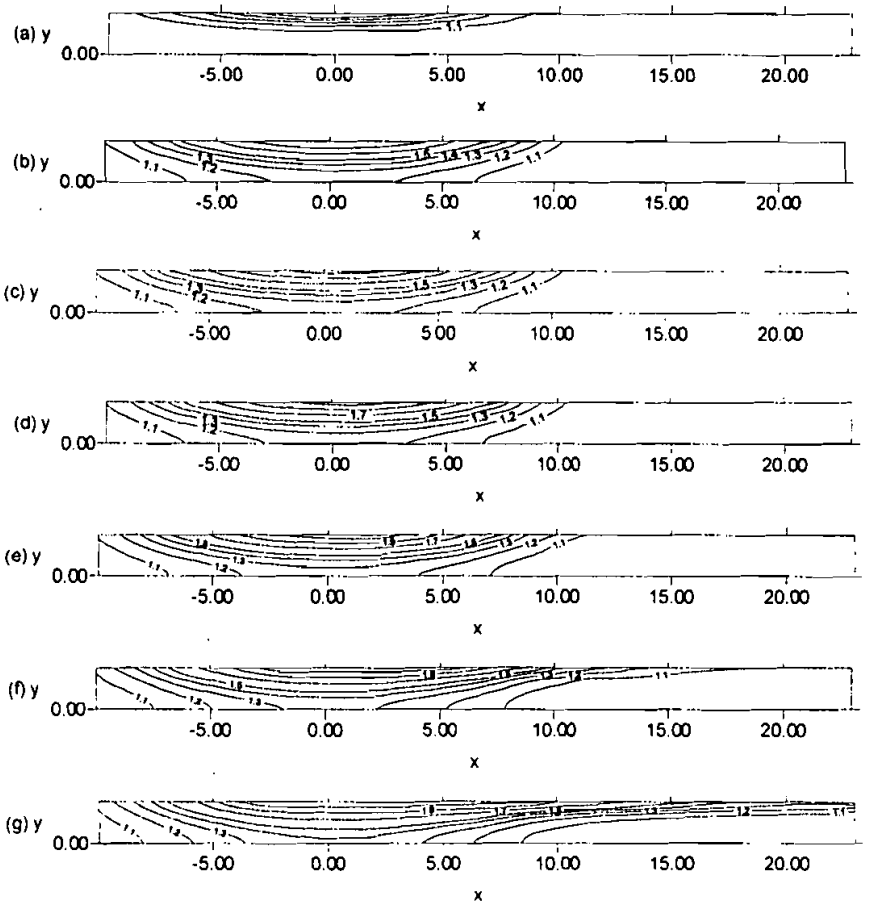


FIGURE 5 Solid fuel temperature distributions for (a) t=190 (b) t=760 (c) t=770 (d) t=780 (e) t=820 (f) t=920 (g) t=1030 (isotherm values, from 1.1 to 1.5, $\Delta T$=0. 1 and then $\Delta T$= 0.2)

decreases slightly with time because of the surface radiation loss (Eq. (9)), which increases with surface temperature. Although the total externally imposed radiative heat, $q_{extt}(= \int_{x=x_{min}}^{x=x_{max}} q_{ext} dx$, remains constant (represented by the thicker horizontal solid line), the total heat flux received, $q_i$, is less than the externally-imposed total heat flux ($q_{extt}$) because of the following factors. The first one is the surface radiation heat loss. The second, the value of $q_{lg}(= \int_{x=x_{min}}^{x=x_{max}} k \left.\frac{\partial T}{\partial y}\right|_{y=\delta_n^+} dx$, the total heat flux received at interface from gas

phase) is negative in the heating up stage, implying that a portion of the energy loses from solid to the ambient to heat the gas phase.

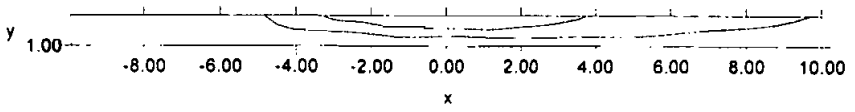


FIGURE 6 Temporal variation of the pyrolysis region at t=760 and 1030

Finally, according to our results, the volatile compounds commence to blow into the gas phase at the later stage (around t=430). Their amount, although insignificant, can generate a flammable mixture near the interface for the following ignition.

The period between t=770 to t=1030 is classified as the ignition process. This period starts from t=770, when ignition initiates. According to Fig. 2, a sharp increase in maximum gas-phase temperature marks this stage. This temperature increases from 2.44 to 9.36 within the period of 260. The average rise is about 1473K/s, much greater than that in the heating up stage.

According to Fig. 3(c), a relatively high temperature contour (T=2.3) in envelope shape is found on the right-hand side of x=0, indicating that the active reaction occurs in gas phase. Figure 7 illustrates the series of flame growing process after ignition, in which the flame is represented by the constant reactivity contour of $10^{-4}$ g/cm$^3$ as mentioned previously. This figure depicts the flame grows very fast from an initially smaller, weaker flame (t = 770) to a much greater, stronger one (t = 1030) within 1.424 seconds in ignition process.

Figures 3 (c) to (g) illustrate this sudden development, or thermal run-away process. Such a development is because the premixed fuel/oxygen mixture, built up in the former stage, has been reacted to gain a higher temperature caused by the heat release in the chemical reaction. Subsequently, the gas phase generates more heat and further accelerates the chemical reactions. This also accounts for why the maximum temperature increases so sharply. At t=1030, the maximum temperature in gas phase reaches 9.36 (Fig. 2), i.e. the highest value found during the ignition process.

For the flow structure in Fig. 3(c) to 3 (g), the sudden gas expansion further accelerates its velocity downstream; the maximum velocities at t=770 and t=920 are 0.739 and 3.474, respectively. At t=1030, the maximum velocity reaches 4.447. The acceleration is quite significant. On the other hand, the same figures indicate that the induced flow ahead of the flame's leading edge is retarded: this is due to the local high-pressure plateau generated by the thermal expansion

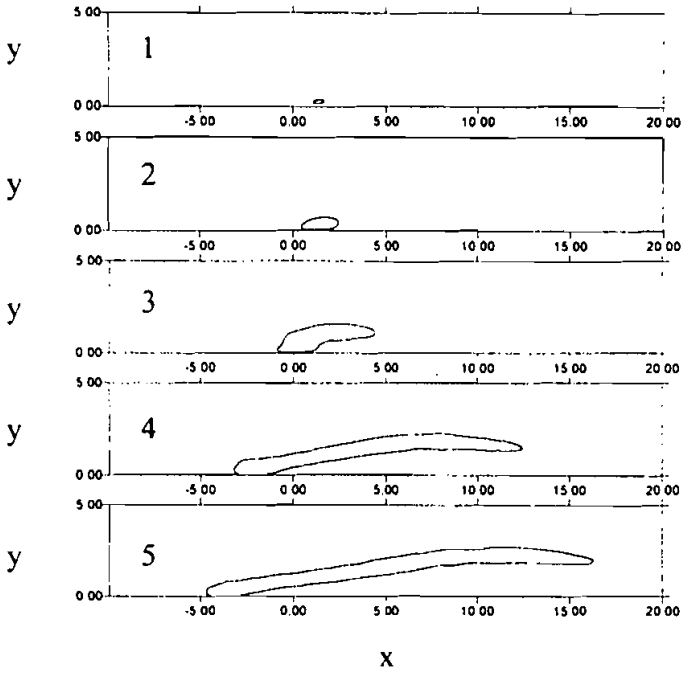


FIGURE 7(A) Constant contour distributions of chemical reaction rate equal to $10^{-4}$ g/cm$^3$.s at various time (1: t=770, 2: t=780, 3: t=820, 4: t=920, 5: t=1030)

attributable to active combustion. Thereafter, this high-pressure plateau accelerates the flow towards downstream.

Figures 4(c) to 4(g) display the transition process in form of fuel/oxidizer mass fraction distributions how the premixed flame becomes the diffusion flame, except in the small upstream region, termed as flame front. In that region, the fuel and oxidizer can leak through the quenching layer between the flame front and solid fuel surface and form the fuel-oxidizer mixture just ahead of the flame front. This mixture serves as a continuous ignition source for the further downward flame propagation.

Figures 5 (c) to 5 (g) illustrate the corresponding temperature distributions in solid phase. According to these figures, the temperature distributions around the upstream flame front are nearly invariant. It is because that the flame is under development and the flame front propagates upstream very slowly due to the retardation by the incoming cold air flow as mentioned above. In the downstream from t=770 (Fig. 5(c)) to t=820 (Fig. 5(e)), the temperature distributions closely resemble each other as well. However, the pyrolysis region starts to extend fur-

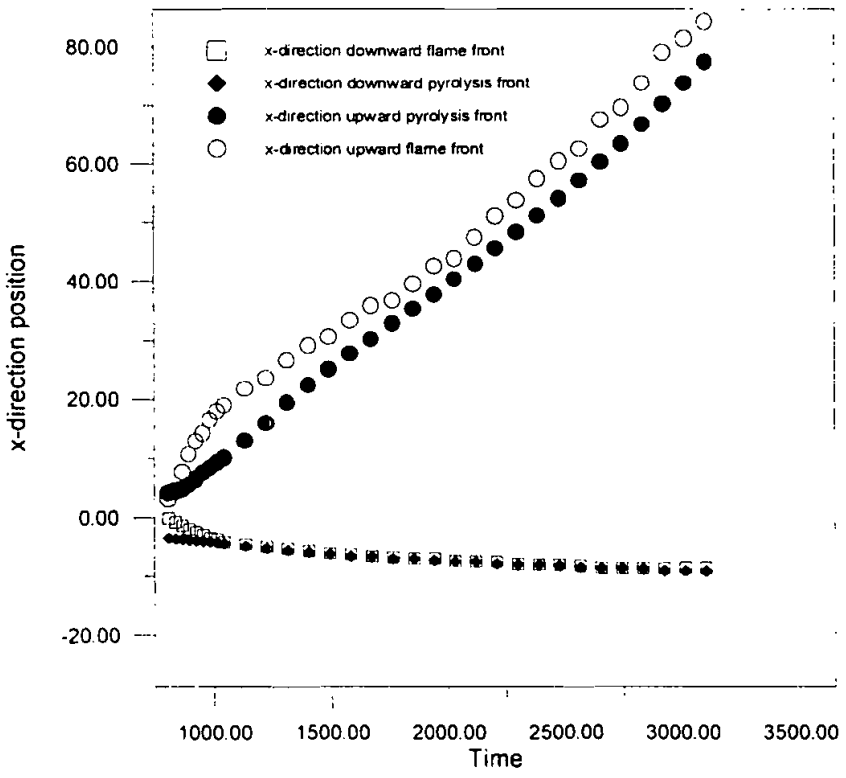


FIGURE 7(B) Upward and downward flame front and pyrolysis front positions

ther downstream in the latter stage of ignition process due to flame extension by the accelerated heat convection (Fig. 6).

In the ignition process, a large amount of heat release in gas phase causes a large feedback of heat to the solid fuel. Instead of heating the gas phase during the heating up stage, the solid fuel begins receiving energy from the gas phase at this stage. Figure 2 depicts the total energy received ($q_i$) by solid fuel increases sharply, as attributed to the following two reasons. The first one is that a rise in gas phase temperature increases the interface temperature gradient, which is directly proportional to conduction heat flux. The other reason is that, since the flame serves as a heat source, the heated length along the interface is lengthened in the spreading process: this is attributed to the amount of total heat flux received. A similar trend also occurs in the total amount of mass flux released.

The transition process comes after the ignition process. This process starts from t=1030, when the maximum temperature decreases from its highest value

as the large amount of premixed mixture consumes almost completely. The flame structures in this stage resemble the ones at t=1030. In addition to the externally imposed heat, the flame now serves as an extra heat source to further pyrolyze the solid fuel to sustain itself. During this process, the maximum temperature decreases to its minimum value 8.18 at t=1840; it then oscillates slightly, increasing again very slowly.

Figure 7(b) depicts the upward and downward flame front and pyrolysis front positions as a function of time. This figure clearly indicates that the upward flame spread rate is much faster than the downward one as time proceeds. This faster rate is owing to that the downward flame spread is against the incoming cold induced flow whereas the upstream one is aided by the accelerated heat convetion. The former one is the so-called opposed flame spread, and the latter one is the concurrent flame spread.

With the continuous existence of externally radiative heat, heat is conducted through the solid continuously and the flame is not strong enough so that the downward pyrolysis front overtakes the flame front for t<1030. This finding apparently suggests that the controlling mechanism is solid conduction. After t=1030, the downward pyrolysis front location is nearly the same as the flame front one, implying that the controlling mechanism of heat transfer mode for downward flame spread now is gas phase conduction. The averaged downward flame spread rate in transition process is 0.058cm/s, i.e. greater than that of the one obtained in a downward flame spread process (=0.0213 cm/s) (Lin and Chen, 1999) by using a steady relative coordinate under a assumption of constant flame spread rate. This greater rate is owing to that the external radiation heat is imposed on the solid surface continuously, whereas there is no such extra heating source in the last work (Lin and Chen, 1999). On the other hand, the hot reacting gases and the post-combustion gases generated in the burning region are carried by the accelerating flow to downstream. As well known, the heat convection in gas phase is much more effective than the solid phase conduction. Therefore, the upward flame front is ahead of its solid fuel pyrolysis front. The averaged upward flame spread rate is 0.65 cm/s from t=1030 to t=1840. After that, the maximum temperature increases and the upward flame spread rate reaches a value of 0.90 cm/s.

Finally, in the transition process, $q_i$, $q_g$, and $m_s$ are still increased with time; however, the acceleration rate decreases significantly. According to Fig. 2, $q_i$ and $q_g$ obviously differ because of the surface re-radiation effect.

## Effect of Changing Externally Radiative Heat Imposed Time

Figure 8 displays the histories of maximum temperature for various heating periods under the same incident heat flux distribution. In Case 1, the externally radi-

ative heat is imposed and maintained for the entire computational time. For Case 2, the incident heat flux is terminated at t=770 and it is at t=1030 for Case 3. This finding indicates that if the incident heat flux does not keep heating the solid fuel after ignition initiation occurs (t=770); no persisting ignition existed. Such an ignition is simply a transient phenomenon because the resultant flame cannot provide sufficient energy to overcome the heat loss and sustain itself into the later stage. On the other hand, if the radiative heat is imposed until the transition process starts, such as Case 1 and Case 3, the flame can sustain itself for persisting ignition. This trend corresponds to the observation in the experimental works of Kashiwagi (1982) and theoretical analysis of Bradley (1970).

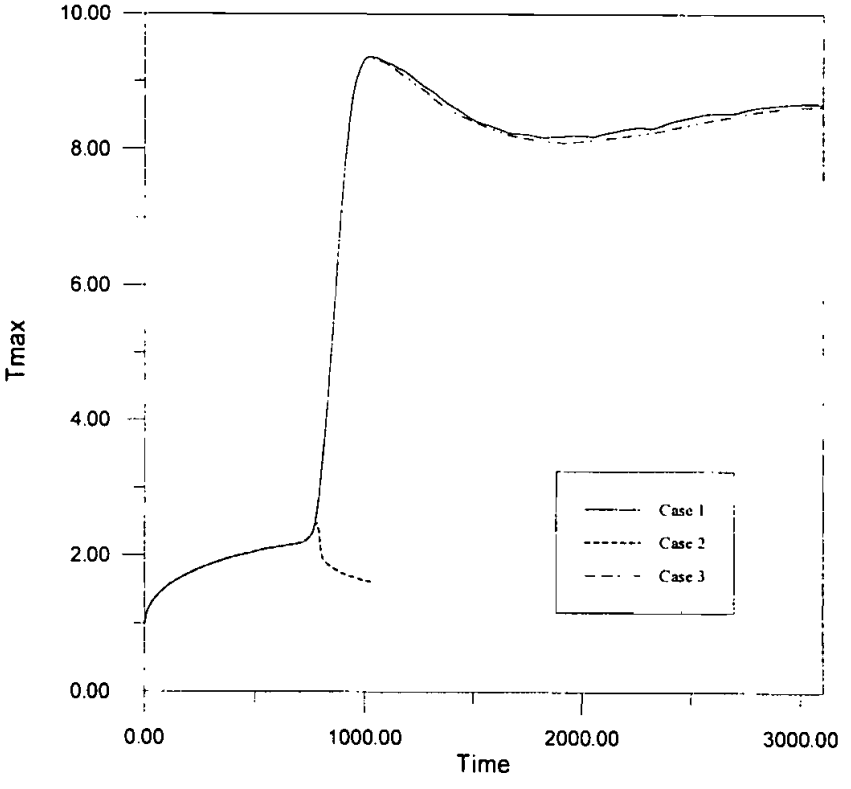


FIGURE 8 Effect of changing externally radiative heat imposed time on ignition behaviors

Case 1 and Case 3 are compared as follows. First, Fig. 8 depicts that the maximum temperatures in Case 1 and 3 decrease from their highest values, reach their lowest ones, and then increase again in the transition process. The lowest maxi-

mum temperature for Case 3 is 8.103 and occurs at t=1900; whereas for Case 1, it is 8.180 and occurs at t=1840. Furthermore, Case 3 has no oscillation phenomenon of maximum temperature, whereas Case 1 does have but with a very small amplitude. This is owing to that the heat diffusion rate inside the solid fuel, which is related to the solid fuel pyrolysis reaction, lags behind the fuel consumption rate in flame. However, there is no such mechanism for Case 3, which has no externally imposed heat flux in transition process. Second, in Case 1, the flame front in the downstream x-direction is −7.57 at t=2200 and −8.72 at t=2950, whereas in Case 3, it is −4.40 and −4.1 at the corresponding time. This observation suggests that the flame front in Case 3 does not propagate against the induced air stream but retreats slightly. Apparently, externally imposed radiative heat after ignition process contributes to extra heating and further enhances the pyrolysis reaction. This accounts for why the flame can spread downward with radiative heat. On the other hand, the flame front moves slightly downstream in Case 3, implying that the flame itself cannot provide enough heat to pyrolyze the upstream solid fuel for downward flame spread to occur at this moment. The downstream flame front location in the x-direction extends to 80.25 at t=2950 for both Case 1 and Case 3. Since the pyrolyzed volatile compounds react in a high temperature near the region in which it is produced, the effect of radiative heat on the downstream flame front location was not so apparent as its effect on the upstream flame front location.

## Effect of Solid Fuel Thickness

Previous studies (Di Blasi, 1994; Lin and Chen, 1999) conferred that solid fuel thickness significantly affects flame spread characteristics. However, the effect of solid fuel thickness on ignition has seldom been investigated in detail. Thus, this work selected a set of solid fuel thickness varying from 0.5 mm (corresponding to 0.360 non-dimensionally) to 5 mm (corresponding to 3.605 non-dimensionally) to examine its influence on ignition behaviors. Table V summarizes the computational results, in which nondimensional ignition delay time (I.D.T), maximum interface temperature at the instant of ignition ($T_{simax}$), and $\delta_c$ are included as well for further discussions. Notably, $\delta_c$ is the dimensionless parameter ($\delta_c = \bar{q}_{ext} \cdot \bar{\delta}_s / k_s(T_{si} - T_{s\infty})$, proposed by Kanury (1995), to distinguish the thermally-thin fuel from thermally-thick one. This parameter can be viewed as the ratio of solid fuel thickness to the thermal penetration depth. Values of $\delta_c$ listed in Table V are based on $\bar{q}_{ext} = 5W/cm^2$, and $T_{si} = 700K$ (the ceiling pyrolysis temperature). Defining $\delta_c$=1 as the dividing criterion for thermally-thin and thermally-thick fuels reveals that a thickness of $\delta_s > 0.721$ can be regarded as a thermally-thick solid fuel when ignition occurs. Otherwise, it is a thermally-thin fuel.

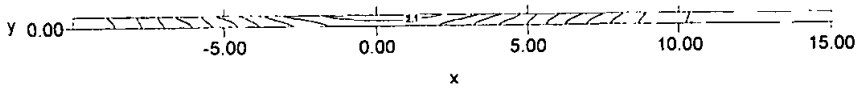


(a) Isotherm values: 2.1 to 1.1 ($\Delta T_s$=0.1)

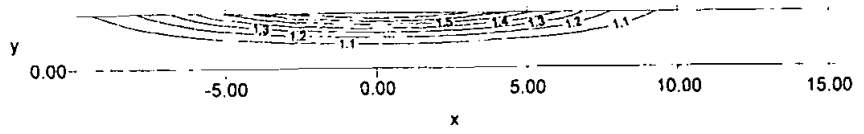


(b) Isotherm values: 1.7 to 1.1 ($\Delta T_s$=0.1)

FIGURE 9 Solid fuel temperature distributions at t=290 for (a) $\delta_s$=0.360 and (b) $\delta_s$=1.802

Table V indicates that the ignition delay time increases with an increase of solid fuel thickness for $\delta_s < 1.802$. Within the domain of $1.802 \leq \delta_s \leq 3.244$, the ignition delay time remains constant. Thereafter, for a solid fuel thickness of $\delta_s$=3.605, the ignition delay time increases slightly. Although ignition delay time varies with solid fuel thickness, this table reveals that the maximum gas-solid interface temperatures at ignition (between 2.25~2.27) are largely unaffected by solid fuel thickness.

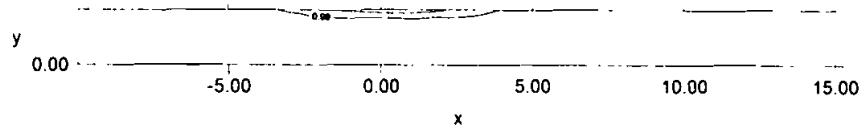


(a) Constant contour values: 0.99,0.9

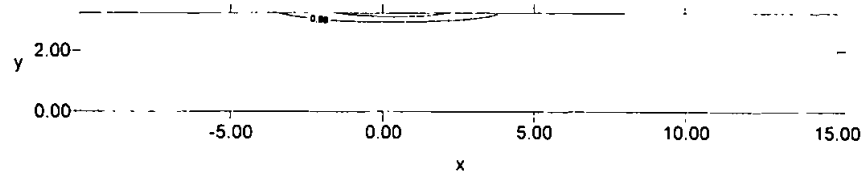


(b) Constant contour values: 0.99,0.9

FIGURE 10 Solid fuel density distributions at $t$=770 for (a) $\delta_s$=1.802 and (b) $\delta_s$=3.244 (peak heat flux value =5W/cm$^2$)

In the heating up stage, the thicker solid fuel requires much more imposed heat than the thinner one to reach the same status as the bottom side is adiabatic. It is

because the larger volumetric heat absorption retards the temperature rise, subsequently slowing down solid fuel pyrolysis. This retardation in a thicker solid fuel also reduces the heat transfer to gas phase because of a less temperature gradient at interface. Therefore, ignition delay time is longer for a thicker solid fuel when subjected to the same imposed heat flux distribution: this can be confirmed by Figs. 9(a) and (b), which show the solid fuel temperature distributions for $\delta_s$=0.360 and 1.802, respectively, at t=290. At that instant, ignition occurs for $\delta_s$=0.360. The maximum temperature at interface for $\delta_s$=0.360 is 2.253 and it is 1.859 for $\delta_s$=1.802. Meanwhile, the non-dimensional maximum heat penetration depth is 0.96 for the latter thickness, indicating that it still behaves as a thermally-thick fuel. Consequently, under the same heat flux exposure, the ignition delay time is longer for $\delta_s$=1.802 than that for $\delta_s$=0.360. However, the computational results indicate that the ignition delay time remains constant for $1.802 \le \delta_s \le 3.244$. This is owing to that the pyrolysis front generated by this incident radiative heat flux (5W/cm$^2$) before the initiation of ignition does not reach the bottom side (Fig. 10) yet for these thermally-thick fuels. Consequently, the solid density profiles are nearly the same and the temperature distributions are somewhat similar for this range of fuel thickness as shown in Figs. 10 and 11. Therefore, as expected, the ignition delay times are not affected by thickness within this range.

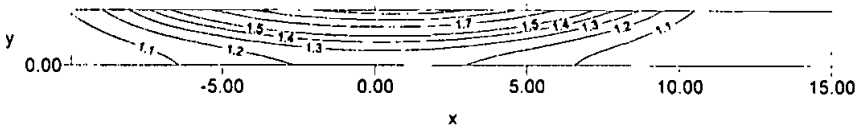


(a) Isotherm values: from 1.1 to 1.5, ΔT= 0.1 and then ΔT= 0.2

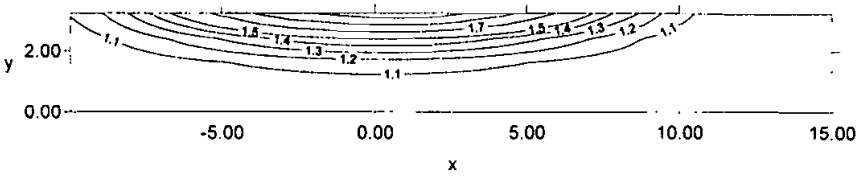


(b) Isotherm values: from 1.1 to 1.5, ΔT= 0.1 and then ΔT= 0.2

FIGURE 11 Solid fuel temperature distributions at $t$=770 for (a) $\delta_s$=1.802 and (b) $\delta_s$=3.244 (peak heat flux value = 5W/cm$^2$)

To examine the relationships between the external heat flux, solid fuel thickness, and ignition delay time, several runs were conducted for varying peak heat flux value, keeping the half-width constant. The peak flux values selected are

6.5W/cm$^2$and 3.5 W/cm$^2$, and the corresponding non-dimensional total heating rates are 39.27 and 21.15, respectively. The non-dimensional total heating rate for peak heat flux value at 5 W/cm$^2$ is 30.21. According to Fig. 12, the relationship between ignition delay time and solid fuel thickness shows a similar trend for peak flux values 5 W/cm$^2$ and 6.5W/cm$^2$. For a peak heat flux value of 3.5 W/cm$^2$, the ignition delay time increases with an increase in solid fuel thickness. While considering the differences between the three heating conditions, this work concludes that if the incident heating rate exceeds the heat diffuse rate within solid fuel, then the heating of solid layer adjacent to the surface is unaffected by solid fuel thickness, assuming that its thickness is greater than the critical value; nor will the pyrolysis reaction. Figure 10 confirms such an effect. On the other hand, if the incident heating rate is the same order as the heat diffuse rate, such as the case of peak heat flux value equal to 3.5 W/cm$^2$, the ignition delay time increases with an increase in solid fuel thickness, for the reason described in the previous paragraph.

## CONCLUSIONS

A theoretical analysis is developed and solved numerically to investigate the ignition behaviors of a vertically oriented cellulosic material subjected to a specified incident heat flux under natural convection conditions in a normal gravitational field. The governing system for gas phase consists of the following components: a set of time-dependent conservation equations for continuity, momentum, energy, and species; an equation of state, an expression of viscosity variation with temperature; and a one-step overall chemical reaction with finite-rate global kinetics. Above equations are coupled with the unsteady solid phase energy and mass conservation equations at the interface.

The ignition and transition to flame spread process over the solid fuel can be divided into two stages: (I) heating up stage, during which the maximum temperature, occurred nearly at interface, is increased with time, but with a decreasing rate, because pyrolysis reaction becomes active in the later stage. In the heating process, the heated region is enlarged and the flammable mixture preparing for the following ignition is generated. Also, the maximum induced flow velocity is increased with time because the increasing temperature gradient. (II) flame development stage, which includes ignition and transition processes. The ignition process is characterized by a sharp increase in maximum temperature. Such an increase is attributed to that a large amount of heat is generated from chemical reaction of the accumulative, flammable mixture. Meanwhile, the flame is in a transition from a premixed flame to a diffusion flame, except in a small region

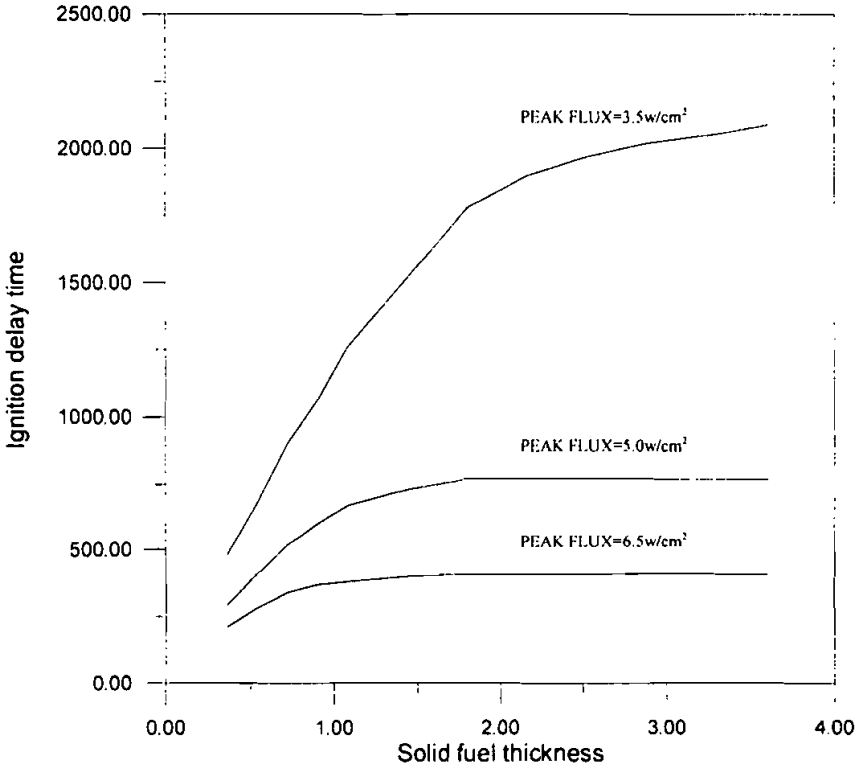


FIGURE 12 Relation between solid fuel thickness and ignition delay time at various external heat flux

just around the flame front. The induced flow ahead of the flame's leading edge is retarded by the local high-pressure plateau, as generated by the thermal expansion attributable to active combustion. Thereafter, this high-pressure plateau accelerates the flow towards downstream. In the transition process, the maximum temperature decreases from the highest value since the large amount of flammable mixture is almost consumed. The flame is fully developed into a diffusion flame except in a small upstream region. In addition to the externally imposed heat, the flame serves as the heat source to pyrolyze the solid fuel further to sustain itself. The observation reveals that the upward flame front travels faster than the downward flame front, because the heat transfer from the flame to the unburnt fuel is rendered more difficult by the gas flow moving against the propagating flame.

Parametric study by varying the imposed radiative heating duration reveals that a longer time for the incident radiative heat flux leads the transition ignition to a persisting ignition. This work also explores the dependency of ignition delay time on solid fuel thickness, varying from $\delta_s$=0.360 to 3.605. Three peak heat flux values (3.5W/cm$^2$, 5W/cm$^2$, and 6.5W/cm$^2$) with the same half width of 1 cm are selected to further explore the effects of solid fuel thickness and external heat flux on solid fuel ignition behaviors. According to the prediction, the ignition delay time increases with an increase of solid fuel thickness when $\delta_s <$ 1.802 for all three peak heat flux values. This occurrence is attributed to that the larger volumetric heat absorption retards the temperature rise in solid fuel, which, in turn, slows down the solid fuel pyrolysis reaction, further delaying ignition. For $1.802 \le \delta_s \le 3.244$, the ignition delay time remains constant for the high and medium peak flux values. In this domain, if the external heating rate is greater than that of the heat diffusion rate inside the solid, then the temperature distributions are similar and the pyrolysis regions are nearly the same. Consequently, the ignition delay times are more or less the same. For the peak flux equal to 3.5W/cm$^2$, the ignition delay time increases with an increase of solid fuel thickness since the external heating rate is the same order as the heat diffusion rate.

## NOMENCLATURE

| | |
|---|---|
| $A_S$ | Non-dimensional pre-exponential factor for fuel pyrolysis $A_s = \overline{A_s}\,\overline{\alpha^*}/\overline{V_r}^2$ |
| $\overline{B}$ | Dimensional pre exponential factor for gas phase reaction |
| C | The specific heat ratio of gas mixture to solid fuel, $C = \overline{C}_p/\overline{C}_s$, |
| $\overline{C}_p$ | Dimensional specific heat for gas mixture |
| $\overline{C}_s$ | Dimensional specific heat for solid fuel |
| $\overline{D}$ | Dimensional species diffusivity |
| Da | Damköhler number, $Da = Y_{O,\infty}\overline{B}\overline{\rho}^*\overline{\delta}/\overline{V}_r$ |
| E | Non-dimensional activation energy for gas phase, $E = \overline{E}/\overline{RT}_\infty$, |

| | |
|---|---|
| $E_s$ | Non-dimensional activation energy for solid phase, $E_s = \overline{E}_s/\overline{R}\overline{T}_\infty$ |
| f | Stoichiometric oxidizer/fuel mass ratio |
| g | Gravitational acceleration, $\overline{g}/\overline{g}_c$ |
| $\overline{g}_c$ | Dimensional normal earth gravity |
| Gr | Grashof number, $\overline{g}(\overline{\rho_\infty} - \overline{\rho_f})\overline{\delta}^3/\overline{\rho}^*\overline{\nu}^{*2}$ |
| $\overline{k}$ | Dimensional gas phase conductivity |
| $k_s$ | Non-dimensional solid phase conductivity, $k_s = \overline{k}_s/\overline{k}^*$ |
| L | Non-dimensional latent heat, $\overline{L}/\overline{C}_s\overline{T}_\infty$ |
| Le | Lewis number, $Le = \overline{\alpha}/\overline{D}$ |
| $m_s''$ | Nondimensional mass flux, $m_s'' = \overline{m}_s''\overline{\alpha}^*/\overline{\rho}_{s\infty}\overline{V}_r^2\overline{\delta}_s$ |
| P | Pressure, $P = (\overline{P} - \overline{P}_\infty)/\overline{\rho}^*\overline{V}_r^2$ |
| Pr | Prandtl number, $\overline{\nu}/\overline{\alpha}$ |
| q | Non-dimensional heat of combustion per unit mass of fuel, $q = \overline{q}/\overline{C}_p\overline{T}_\infty$ |
| $q_{ext}$ | Non-dimensional external heat flux, $q_{ext} = \overline{q}_{ext} \cdot \overline{\delta}/k^* \cdot \overline{T}_\infty$ |
| $\overline{R}$ | Dimensional universal gas constant |
| t | Non-dimensional time, $t = \overline{t}\overline{V}_r/\overline{\delta}$ |
| T | Non-dimensional gas phase temperature, $\overline{T}/\overline{T}_\infty$ |
| $T_s$ | Non-dimensional solid phase temperature, $\overline{T}_s/\overline{T}_\infty$ |
| u | Non-dimensional velocity parallel to the fuel surface, $u = \overline{u}/\overline{V_r}$ |
| V | Non-dimensional velocity normal to the fuel surface, $v = \overline{v}/\overline{V_r}$ |
| $\overline{V}_r$ | Reference velocity, $[\overline{g} \cdot (\overline{\rho}_\infty - \overline{\rho}_f) \cdot \overline{\alpha}^*/\overline{\rho}^*]^{1/3}$ |
| $\dot{\omega}_F$ | Non-dimensional reaction rate |

| | |
|---|---|
| x | Non-dimensional distance parallel to the fuel surface, $\overline{x}/\overline{\delta}$ |
| y | Non-dimensional distance normal to the fuel surface, $\overline{y}/\overline{\delta}$ |
| $Y_F$ | Fuel mass fraction |
| $Y_O$ | Oxygen mass fraction |
| Greek Symbols | |
| $\overline{\alpha}$ | Dimensional thermaldiffusivity |
| $\alpha_s$ | Non-dimensional thermal diffusivity, $\alpha_s = \overline{\alpha_s}/\overline{\alpha}$ |
| $\overline{\delta}$ | Reference length |
| $\delta_s$ | Non-dimensional solid fuel thickness, $\overline{\delta}_s/\overline{\delta}$ |
| $\mu$ | Non-dimensional dynamic viscosity, $\mu = \overline{\mu}/\overline{\mu}^*$ |
| $\rho$ | Non-dimensional density of gas phase, $\rho = \overline{\rho}/\overline{\rho}^*$ |
| $\rho_S$ | Non-dimensional density of solid phase, $\rho_s = \overline{\rho}_s/\overline{\rho}_{s\infty}$ |
| $\sigma$ | Stefan-Boltzmann constant, $\sigma = \overline{\sigma} \cdot \overline{\delta} \cdot \overline{T}_\infty^3/k^*$ |
| $\gamma$ | Temperature ratio, $\overline{T^*}/\overline{T_\infty}$ |
| $\overline{\nu}$ | Dimensional kinematic viscosity |
| $\varepsilon$ | surface emittance (=1) |
| overhead | |
| $\overline{\ }$ | Dimensional quantities |
| Superscript | |
| " | flux |
| * | reference state on $\overline{T}^*$ |
| Subscript | |
| f | Flame |
| i | Interface |
| max | Location of downstream boundary |
| min | Location of upstream boundary |
| S | Solid phase |
| sf | Char |

| | |
|---|---|
| V | Ceiling pyrolysis temperature |
| ∞ | Ambient condition |

## Acknowledgements

The authors would like to thank the National Science Council of Taiwan, R.O.C., for financially supporting this research under Contract No. NSC88–2212-E009–017



## References

Altenkirch, R. A., Eichhorn, R., and Shang, P. C., (1980) Buoyancy effects on flame spreading down thermally thin fuels, *Combust. Flame.*, 37, 71–83.

Alvares, N. J., and Martin, S. B., (1971) Mechanisms of ignition of thermally irradiated cellulose, *Thirteenth Symposium (International) on Combustion, The Combustion Institute*, 905–914.

Amos, B. and Fernandez-Pello, A. C., (1988) Model of the ignition and flame development on a vaporizing combustible surface in a stagnation point flow: ignition by vapor fuel radiation absorption, *Combust. Sci. Technol.*, 62, 331–343.

Bradley H. H., JR, (1970) Theory of ignition of a reactive solid by constant energy flux, *Combust. Sci. Technol.*, 2, 11–20.

Di Blasi, C., (1988) Near limit flame spread over thick fuels in a concurrent forced flow, *Combust. Flame.*, 72, 205–215.

Di Blasi, C., (1994) Processes of flame spreading over the surface of charring fuels: effects of the solid thickness, *Combust. Flame.*, 97, 225–239.

Duh, F. C. and Chen C.H., (1991) A theory for downward flame spread over a thermally-thin fuel, *Combust. Sci. Technol.*, 77, 291–305.

Fernandez-Pello, A.C. (1995) The solid phase. In Cox, G., Combustion fundamentals of fire, academic press inc., San Diego, chap. 2, pp. 34–100.

Gandhi, P. D. and Kanury A. M., (1988) Thesholds for spontaneous ignition of organic solids exposed to radiant heating, *Combust. Sci. Technol.*, 57, 113–128.

Kashiwagi, T., (1974 ) A radiative ignition model of a solid fuel, *Combust. Sci. Technol.*, 8, 225–236.

Kashiwagi, T., (1979 a) Experimental observation of radiative ignition mechanisms, *Combust. Flame.*, 34, 231–244.

Kashiwagi, T.,(1979 b) Effect of attenuation of radiation on surface temperature for radiative ignition, *Combust. Sci. Technol.*, 20, 225–234.

Kashiwagi, T., (1981) Radiative ignition mechanism of solid fuels, *Fire Safety J.*, 34, 185–200.

Kashiwagi, T., (1982) Effects of sample orientation on radiative ignition, *Combust. Flame.*, 44, 223–245.

Kanury, A. M., (1995) *The SFPE HANDBOOK of Fire Prot. Eng.*, section 2, chapter 13, 190–204.

Kindelan, M., and Williams, F.A., (1977) Gas-phase ignition of a solid with in-depth absorption of radiation, *Combust. Sci. Technol.*, 16, 47–58.

Lin, Pei-Hsun, (1998) Proposal for Ph.D dissertation, Department of Mechanical Engineering, National Chiao-Tung University, Hsin Chu, Taiwan 300.

Lin, P. H. and Chen, C. H., (1999) Numerical analyses for downward flame spread over thin and thick fuels in gravational field, accepted by *Combust. Flame.*

Mcgrattan K.B., Kashiwagi T., Baum H.R. and Olson S.L., (1996) Effect of ignition and wind on the transition to flame spread in a microgravity environment, *Combust. Flame.*, 106, 377–391.

Martin, S.B., (1965), Basic studies of the mechanism of ignition of cellulosic materials, *Tenth Symposium (International) on Combustion, The Combustion Institute*, 877–896.

Nakabe K., Mcgrattan K.B., Kashiwagi T., Baum H.R., Yamashita H., and Kushida G., (1994) Ignition and transition to flame spread over a thermally thin cellulosic sheet in a microgravity environment, *Combust. Flame*, 98, 361–374.

National Bureau of Standards (US) (1955), *Table of properties of air at atmospheric pressure. Circular* 564.

Patankar, S. V., (1980) *Numerical Heat Transfer and Fluid Flow*, Hemisphere, London.

Suzuki, M., Dobashi, R., and Hirano, T., (1994) Behavior of fires spreading downward over thick paper, *Twenty-Fifth Symposium (International) on Combustion, The Combustion Institute*, 1439–1446.

West, J., and Bhattacharjee, S., (1992) A comparison of the roles played by natural and forced convection in opposed-flow flame spreading, *Combust. Sci. Technol.*, 83, 233–244.